7
Implications of strong magnetic fields on exotic dense matter equation of state

7.1 Introduction

As mentioned earlier in chapter-1, among the remarkable features of compact stars are the wide range of densities covered by their interiors (from sub-saturation up to possibly 10 times the nuclear saturation density) and the huge magnetic field range 10^9 to 10^{18} G. Compact stars are divided in various classes according to some of their characteristic features. These include millisecond pulsars, NSs in X-ray binaries, radio pulsars, anomalous X-ray pulsars, soft gamma repeaters, etc. Among these, the anomalous X-ray pulsars and soft gamma repeaters are believed to be compact stars with the surface magnetic field in the range of 10^{14}–10^{15} G [Harding and Lai, 2006; Turolla et al., 2015] and are commonly referred as *magnetars*. Furthermore, there has been recently growing evidence that (at least) the repeating fast radio bursts (FRBs) are related to magnetars [Margalit et al., 2020; Beniamini et al., 2020; Beloborodov, 2020; Levin et al., 2020; Zanazzi and Lai, 2020]. Since the gravitational equilibrium of compact stars allows stars with magnetic fields in the range $B \leq (2-3) \times 10^{18}$ G [Shapiro and Teukolsky, 1983], large magnetic fields beyond those currently inferred have been studied theoretically. Earlier works [Chakrabarty et al., 1997; Bandyopadhyay et al., 1997; Broderick et al., 2000; Chen et al., 2007; Rabhi et al., 2008] have studied the effects of the magnetic field on the gross parameters of compact stars, such as the mass, radius, moment of inertia under intense magnetic fields. The induced deformations of the NSs due to the strong magnetic fields can be important sources of gravitational waves and precession in NSs. The readers can see refs.-Mallick and Schramm [2014]; Bonazzola et al. [1993]; Bocquet et al. [1995]; Cardall et al. [2001]. The structure of magnetized compact stars, in particular, their deformation, in general relativity, has been studied initially in refs.-Bonazzola et al. [1993]; Bocquet et al. [1995]; Cardall et al. [2001] assuming various forms of the poloidal and toroidal field configurations. More recent studies [Ciolfi et al., 2009, 2010; Ciolfi and Rezzolla, 2013] considered also a combination of toroidal and poloidal fields which appear to be more stable than purely poloidal or toroidal configurations.

Moreover, a "universal" field profile represented by an 8th-order polynomial as a function of star's internal radius has been proposed recently to describe the magnetic field profile inside the star [Chatterjee et al., 2019] based on the solution of Einstein–Maxwell equations in general relativity. While large magnetic fields are required to affect the EoS and the structure of the star, the role of the magnetic field is still important at lower values. In particular, MeV-

scale magnetic field can significantly alter the quasiparticle spectrum of baryons, leading to the suppression of the superfluidity of protons via Landau diamagnetism [Sinha and Sedrakian, 2015; Sinha and Sedrakian, 2015] and superfluidity of neutrons via Pauli paramagnetism [Stein et al., 2016], the readers can see Sedrakian et al. [2017] for a review. These modifications alter the neutrino emissivity of compact stars with MeV-scale magnetic fields [Sinha and Sedrakian, 2015] through the modifications of the neutrino production reaction rates. The anisotropy introduced by the magnetic field also affects evolutionary processes in compact stars such as their magneto-thermal evolution [Pons et al., 2009] and rotational dynamics [Pons and Viganò, 2019; Sedrakian, 2016].

In this work, we study baryonic matter under an intense magnetic field within the framework of RMF theory with density-dependent DD-ME2 parametrization. This chapter is based on the works Thapa et al. [2020, 2022] and is organized as follows. The RMF formalism in the presence of strong magnetic fields is briefly discussed in sec.-7.2 followed by the coupling parameters and magnetic field profiles implemented in this work in secs.-7.3, 7.4 respectively. The results are shown in sec.-7.5 and our conclusions are collected in sec.-7.6.

7.2 Formalism

In this work, we consider matter composed of the full baryon octet, the quartet of Δ-resonances and leptons—electrons and muons (e^-, μ^-). The strong interaction between (non-strange) baryons is mediated by the σ, ω and ρ-mesons. In addition, the hidden strangeness mesons σ^* (scalar) and ϕ (vector) mediate the hyperon–hyperon interactions. The total Lagrangian density of the fermionic component of matter in presence of a magnetic field is given by,

$$\mathcal{L} = \mathcal{L}_m + \mathcal{L}_f, \tag{7.1}$$

where, $\mathcal{L}_m$ and $\mathcal{L}_f$ are the matter and the gauge field contributions, respectively.

We consider the matter part of the Lagrangian density as [Cai et al., 2015; Tolos et al., 2017],

$$\begin{aligned}
\mathcal{L}_m =& \sum_b \bar{\psi}_b (i\gamma_\mu D^\mu - m_b + g_{\sigma b}\sigma + g_{\sigma^* b}\sigma^* - g_{\omega b}\gamma_\mu \omega^\mu - g_{\phi b}\gamma_\mu \phi^\mu - g_{\rho b}\gamma_\mu \boldsymbol{\tau}_b \cdot \boldsymbol{\rho}^\mu)\psi_b \\
&+ \sum_\Delta \bar{\psi}_{\Delta\nu} (i\gamma_\mu D^\mu - m_\Delta + g_{\sigma\Delta}\sigma - g_{\omega\Delta}\gamma_\mu \omega^\mu - g_{\rho\Delta}\gamma_\mu \boldsymbol{\tau}_\Delta \cdot \boldsymbol{\rho}^\mu)\psi^\nu_\Delta \\
&+ \frac{1}{2}(\partial_\mu \sigma \partial^\mu \sigma - m_\sigma^2 \sigma^2) + \frac{1}{2}(\partial_\mu \sigma^* \partial^\mu \sigma^* - m_{\sigma^*}^2 \sigma^{*2}) - \frac{1}{4}\omega_{\mu\nu}\omega^{\mu\nu} + \frac{1}{2}m_\omega^2 \omega_\mu \omega^\mu \\
&- \frac{1}{4}\phi_{\mu\nu}\phi^{\mu\nu} + \frac{1}{2}m_\phi^2 \phi_\mu \phi^\mu - \frac{1}{4}\boldsymbol{\rho}_{\mu\nu} \cdot \boldsymbol{\rho}^{\mu\nu} + \frac{1}{2}m_\rho^2 \boldsymbol{\rho}_\mu \cdot \boldsymbol{\rho}^\mu \\
&+ \sum_l \bar{\psi}_l (i\gamma_\mu D^\mu - m_l)\psi_l
\end{aligned} \tag{7.2}$$

where $D^\mu = \partial^\mu + ieQA^\mu$ is the covariant derivative, A^μ is the electromagnetic vector potential, eQ is the charge of the particle (e being unit '+' charge), the b-summation in the first line is over the nucleons and hyperons (spin-1/2), Δ-summation in the second line is over the Δ-resonances (spin-3/2) and the l summation in the last line is over leptons. The fields ψ_b, ψ_l and ψ^ν_Δ correspond to the Dirac baryons, leptons and the Rarita–Schwinger fields for Δ-resonances.

The electro-magnetic field Lagrangian density in eq.-(7.1) has the standard form

$$\mathcal{L}_f = -\frac{1}{16\pi} F_{\mu\nu} F^{\mu\nu} \tag{7.3}$$

with $F^{\mu\nu}$ being the electro-magnetic field tensor. Below, we adopt the reference frame in which the four-vector potential has the form $A^\mu \equiv (0, -yB, 0, 0)$, where B is the magnitude of the magnetic field.

The field equations incorporated in this framework are already described in chapter-4. The scalar density, baryon number density and the kinetic energy density of the uncharged baryon (denoted by index u) at zero temperature are given by,

$$\begin{aligned}
n_u^s &= \frac{2J_u+1}{2\pi^2} m_u^* \left[p_{F_u} E_{F_u} - m_u^{*^2} \ln\left(\frac{p_{F_u} + E_{F_u}}{m_u^*} \right) \right], \\
n_u &= (2J_u+1) \frac{p_{F_u}^3}{6\pi^2}, \\
\varepsilon_u &= \frac{2J_u+1}{2\pi^2} \left[p_{F_u} E_{F_u}^3 - \frac{m_u^{*^2}}{8} \left(p_{F_u} E_{F_u} + m_u^{*^2} \ln\left(\frac{p_{F_u} + E_{F_u}}{m_u^*} \right) \right) \right],
\end{aligned} \tag{7.4}$$

respectively, where, J_u, p_{F_u}, m_u^*, E_{F_u} are the spin, Fermi momentum, effective mass and Fermi energy of the u th-uncharged baryon. Due to the inclusion of magnetic fields, the same quantities for a charged baryon (denoted by index c) are given by the following expressions:

- Spin-1/2 case:

$$\begin{aligned}
n_c^s &= \frac{e|Q|B}{2\pi^2} m_c^* \sum_{\nu=0}^{\nu_{max}} (2 - \delta_{\nu,0}) \ln\left(\frac{p_{F_c} + E_{F_c}}{\sqrt{m_c^{*^2} + 2\nu e|Q|B}} \right), \\
n_c &= \frac{e|Q|B}{2\pi^2} \sum_{\nu=0}^{\nu_{max}} (2 - \delta_{\nu,0}) p_{F_c}, \\
\varepsilon_c &= \frac{e|Q|B}{2\pi^2} \sum_{\nu=0}^{\nu_{max}} (2 - \delta_{\nu,0}) \left[p_{F_c} E_{F_c} + \left(m_c^{*^2} + 2\nu e|Q|B \right) \ln\left(\frac{p_{F_c} + E_{F_c}}{\sqrt{m_c^{*^2} + 2\nu e|Q|B}} \right) \right],
\end{aligned} \tag{7.5}$$

- Spin-3/2 case:

$$\begin{aligned}
n_c^s &= \frac{e|Q|B}{2\pi^2} m_c^* \sum_{\nu=0}^{\nu_{max}} (4 - \delta_{\nu,1} - 2\delta_{\nu,0}) \ln\left(\frac{p_{F_c} + E_{F_c}}{\sqrt{m_c^{*^2} + 2\nu e|Q|B}} \right), \\
n_c &= \frac{e|Q|B}{2\pi^2} \sum_{\nu=0}^{\nu_{max}} (4 - \delta_{\nu,1} - 2\delta_{\nu,0}) p_{F_c}, \\
\varepsilon_c &= \frac{e|Q|B}{2\pi^2} \sum_{\nu=0}^{\nu_{max}} (4 - \delta_{\nu,1} - 2\delta_{\nu,0}) \left[p_{F_c} E_{F_c} + \left(m_c^{*^2} + 2\nu e|Q|B \right) \ln\left(\frac{p_{F_c} + E_{F_c}}{\sqrt{m_c^{*^2} + 2\nu e|Q|B}} \right) \right],
\end{aligned} \tag{7.6}$$

where, p_{F_c}, m_c^*, E_{F_c} are the Fermi momentum of the ν^{th}-Landau level, effective mass and Fermi energy of the c^{th}-charged baryon. The Landau levels for spin-1/2, 3/2 baryons are denoted by ν, the maximum value of which is defined by,

$$\nu_{max} = \text{Int}\left(\frac{p_{F_c}}{2e|Q|B} \right). \tag{7.7}$$

In the case of spin-1/2 particles, the lowest Landau level has degeneracy equal unity and all other levels have degeneracy equal 2 [Sinha et al., 2013]. In the case of spin-3/2 particles, the degeneracy of the lowest (first) level is 2, for the second level it is 3 and is 4 in the remaining Landau levels [de Paoli et al., 2013].

For the case of leptons ($l \equiv e^-, \mu^-$), the number density and contribution to the kinetic energy density is given by,

$$n_l = \frac{e|Q|B}{2\pi^2} \sum_{\nu=0}^{\nu_{max}} (2 - \delta_{\nu,0}) p_{F_l}, \tag{7.8}$$

$$\varepsilon_l = \frac{e|Q|B}{2\pi^2} \sum_{\nu=0}^{\nu_{max}} (2 - \delta_{\nu,0}) \left[p_{F_l} E_{F_l} + \left(m_l^2 + 2\nu e|Q|B\right) \ln \left(\frac{p_{F_l} + E_{F_l}}{\sqrt{m_l^2 + 2\nu e|Q|B}} \right) \right], \tag{7.9}$$

where, p_{F_l}, m_l, E_{F_l} are the Fermi momentum of the ν th-Landau level, bare mass and Fermi energy of the lepton, respectively.

In eqs.-(7.4)–(7.6), the Fermi momenta p_{F_u} and p_{F_c} are defined as,

$$p_{F_u} = \sqrt{E_F^2 - m^{*^2}}, \quad p_{F_c} = \sqrt{E_F^2 - (m^{*^2} + 2\nu e|Q|B)}, \tag{7.10}$$

with E_F being the Fermi energy of the respective particle.

The energy density and matter pressure expressions are similar to eqs.-(4.11) and (4.13) respectively.

7.3 Coupling parameters

The coupling parameter set implemented in this work is similar to the one as mentioned in chapter-4. The readers can see sec.-4.3 for a comprehensive insight of the considered parametrization and hyperon potentials. In case of Δ optical potentials, we have considered in this chapter the case with $R_{\sigma\Delta} = 1.16$.

7.4 Magnetic field profiles

To model the magnetic field profile in the NS interior, we adopted two types of profiles which give the dependence of the field on the position inside the star.

The *exponential profile* is given by [Bandyopadhyay et al., 1997]

$$B\left(\frac{n_b}{n_0}\right) = B_s + B_c \left\{ 1 - \exp\left[-\beta \left(\frac{n_b}{n_0} \right)^{\gamma} \right] \right\}, \tag{7.11}$$

where B_s and B_c denote the magnetic fields at surface and at center of the star, respectively. The free parameters β and γ are commonly adjusted such as to have a fixed surface magnetic field of 10^{15} G for any given value of the field in the center, which is typically larger than the surface field.

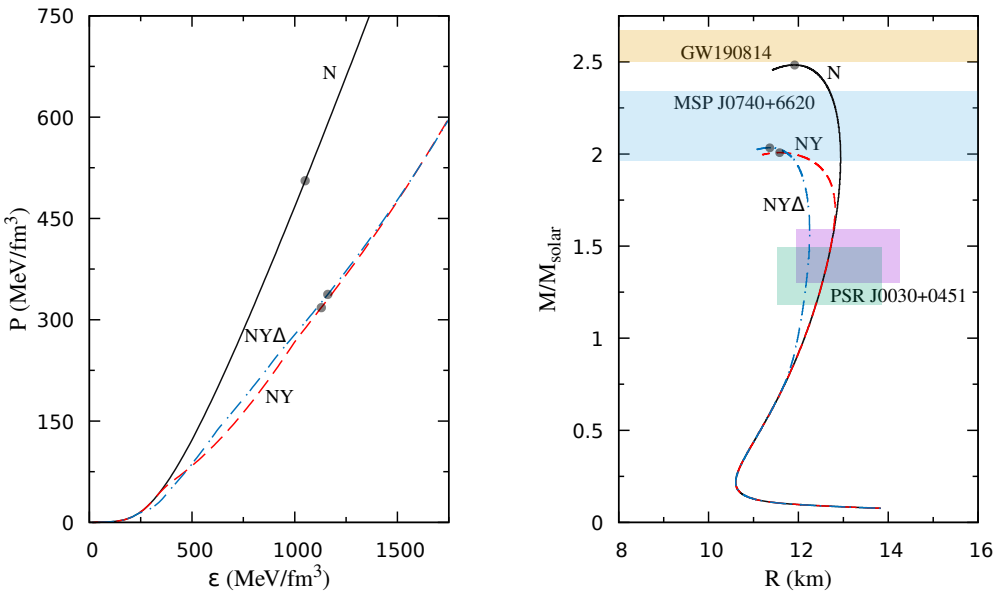

Figure 7.1: Left panel: EoS of matter in the absence of magnetic field for three compositions considered. Solid, dashed, dash-dotted lines correspond to the cases of nucleons only (N), nucleons and hyperons (NY), nucleons, hyperons and Delta (NYΔ), respectively. The circles indicate the location of the maximum mass star for each composition. Right panel: the mass–radius (M–R) relations corresponding to the EoS on the left panel obtain through solutions of the TOV equations. The mass constraints from the various astrophysical observations are represented by the colored bands and correspond to the GW190814 event [Abbott et al., 2020b], MSP J0740+6620 [Cromartie et al., 2020] and the mass–radius limits inferred for PSR J0030+0451 from the NICER experiment [Miller et al., 2019; Riley et al., 2019].

The *universal profile* is given as [Chatterjee et al., 2019]

$$B(x) = B_c \left(1 - 1.6x^2 - x^4 + 4.2x^6 - 2.4x^8\right), \tag{7.12}$$

where $x = r/r_{\rm mean}$, r is the internal radius joining the center to the point of observation, $r_{\rm mean}$ is the mean radius of the star and B_c is the value of the field at the center of the star.

7.5 Results and discussion

In this section, the numerical results of our study are described considering the effect of strong magnetic field on high density stellar matter with three types of composition:

(1) Nucleons (N),

(2) nucleons and hyperons (NY),

(3) nucleons, hyperons and Δ-resonances (NYΔ).

Fig.-7.1 shows the EoS and mass–radius relations for these three compositions of matter in the case $B = 0$ along with some astrophysical constraints on the masses and radii of compact

Table 7.1: Parameter values of the maximum-mass stars for non-magnetic stellar sequences derived for three different compositions. Here, $M_{\rm max}$, R, ε_c denote the maximum mass, corresponding radius and central energy density, respectively.

Composition	$M_{\rm max}$ $(M_\odot)$	R (km)	ε_c (MeV/fm^3)
N	2.483	11.941	1035.558
NY	2.008	11.606	1119.700
NYΔ	2.034	11.365	1161.771

Table 7.2: The values of the energy–density, pressure and number density at the center of non-magnetized stellar models which were used to obtain the universal relation (7.12) as a function of density (instead of the internal radius). We also list the mass and the radius for each model.

Composition	$M(M_\odot)$	R (km)	ε_c (MeV/fm^3)	p_c (MeV/fm^3)	n_c (fm^{-3})
N	2.482	12.002	1000	467.44	0.788
NY	2.000	11.801	1000	266.94	0.846
NYΔ	2.034	11.376	1150	333.38	0.944

stars. Table-7.1 lists some parameters of the stars with maximum masses along the stellar sequences for the three compositions listed above.

Next, we shall discuss the stellar configurations with magnetic field. In order to show the effect of the field in the case of *universal profile*, we need a relation between the internal radius and the density, *i.e.*, the function $r(n)$. This requires us to specify a stellar model. We, therefore, chose three stars from the stable region of M–R curve with parameters shown in table-7.2. After fixing the value of the central field $B_c = 2.9 \times 10^{18}$ G, we are then able to use eq.-(7.12). We note that the predicted surface magnetic field values are $B_s \approx 5.6 \times 10^{17}$ G.

In the case of *exponential profile* (eq.-(7.11)), the surface field is fixed at $B_s = 10^{15}$ G and we adopt the parameter values $\beta = 0.01$ and $\gamma = 3.95,\ 3.15$ and 3.2 for N, NY and NYΔ matter, respectively. The resulting magnetic field profiles guarantee that the matter remains stable under the influence of strong B-field. The stability criteria here denotes the thermodynamic stability one with $dP/d\varepsilon\ > 0$ *i.e.* monotonous increase of matter pressure with energy density as pointed out in Ref.-[Sinha et al., 2013].

Fig.-7.2 shows the ratio of fractions of different species $\delta Y_i = n_i(B)/n_i(0)$ as a function of normalized baryon number density. The oscillating nature of the fractions arises due to successive occupation of Landau levels for the charged species. The effect of the field is not substantial in the low-density regime for exponential field profile as the field strength in this case is small near the surface. In the case of the universal profile, the low-density regime shows strong fluctuations because the decay of the magnetic field with density is small and the surface magnetic field is of the order few times of 10^{17} G. It is interesting to note that for most of the particles $\delta Y_i > 1$, but in the case of Δ^-, the opposite is the case. This is a consequence of the charge neutrality. Due to the Landau quantization the fraction of electrons increases compared to non-magnetic case which causes the Δ^- fraction to decrease. The pattern in fig.-7.2 results from the complicated interplay between the Landau quantization for charge particles entering into the two key conditions imposed—the charge neutrality and baryon number conservation,

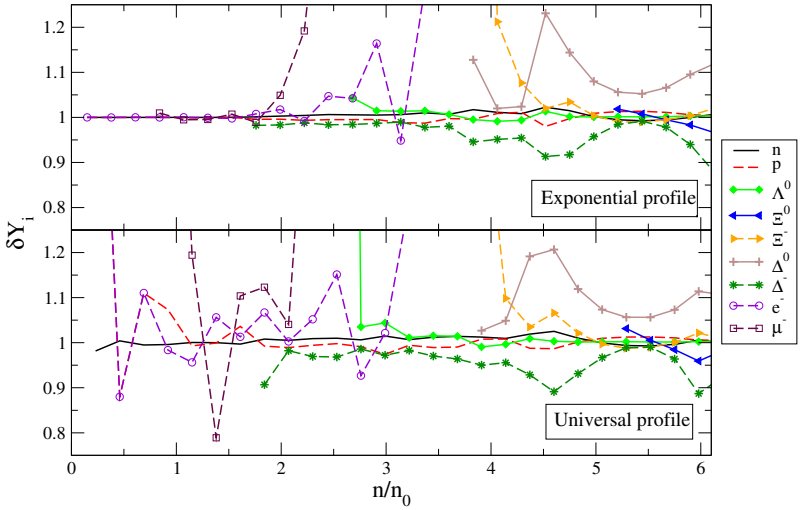

Figure 7.2: Dependence of the ratio $\delta Y_i = n_i(B)/n_i(0)$ on the baryon number density normalized to the nuclear saturation density n_0 for neutrons (n), protons (p), Λ^0, Ξ^0, Ξ^-, Δ^0, Δ^-, e^- and μ^-. The particle markers are indicated in the panel on the right. The upper panel corresponds to the exponential field profile, the lower one to the universal field profile.

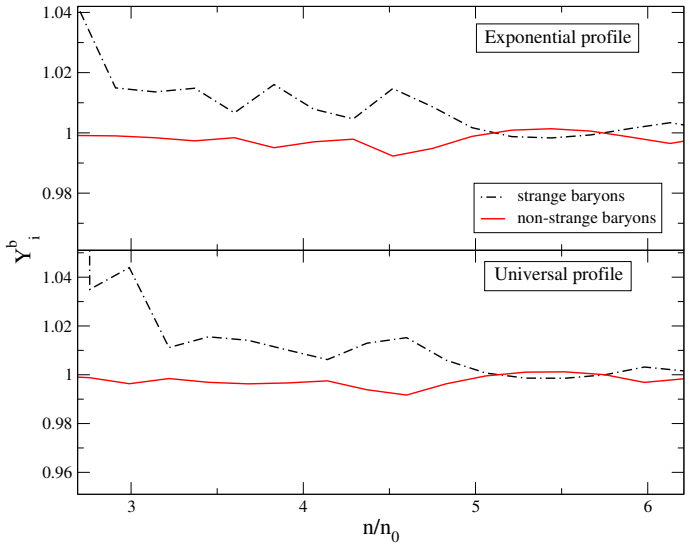

Figure 7.3: The ratio Y_i^b of the partial fractions of strange or non-strange baryons in presence of a magnetic field to that without a magnetic field as a function of baryon number density, n in units of n_0 in the case of $NY\Delta$ composition. Upper panel corresponds to the exponential field profile, the lower panel to the universal field profile.

which are used in the construction of the EoS. Note also that Δ^+ and Δ^{++} resonances do not appear until baryon density of $n \geq 6.1 n_0$ for our particular choice of Δ-potential.

In fig.-7.3 we show the quantity Y_i^b, which is defined as the ratio of the partial fractions of strange or non-strange baryons in presence of a magnetic field to that without a magnetic field. The fraction of strange baryons is affected significantly ($\sim$4%) by the magnetic field, whereas the fraction of the non-strange baryons is affected much less. We see that in the

presence of magnetic field strange baryons appear earlier than in the non-magnetic case. This is, again, a consequence of complex interplay between the imposed charge neutrality condition and modifications of the phase-space occupation due to the Landau quantization.

Finally, to quantify the variations of the effective mass of a baryon in the presence of magnetic field, we show in fig.-7.4 the ratio of effective nucleon Dirac mass (m_N^*) in the magnetic field to its value in the absence of the field $X_{m_n^*} = m_N^*(B)/m_N^*(0)$. It is seen that, for the exponential profile case, m_N^* remains unchanged until the appearance of Δ^- around 1.3 times nuclear saturation density. A similar trend is observed for the universal profile case, but the amplitudes of the oscillations are larger. This is (again) due to the fact that the magnetic field value at the surface of the star is larger for this profile. With the onset of Ξ^-, we observe a reduction in $X_{m_n^*}$ by about 4% in the density range ∼4–5 times saturation density for both the profiles.

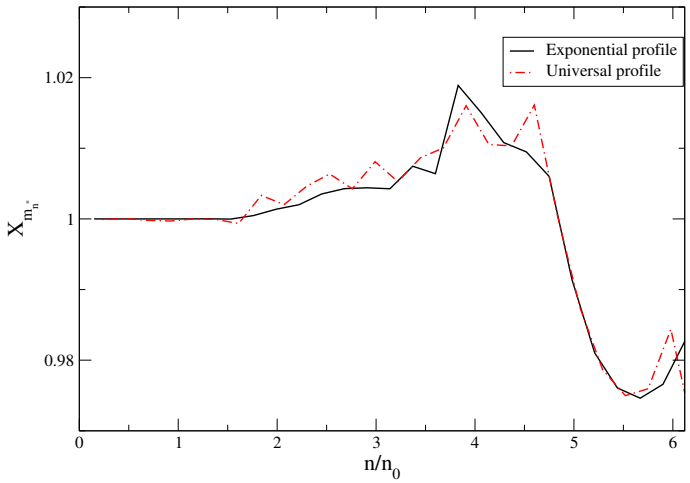

Figure 7.4: Dependence of the ratio $X_{m_n^*} = m_N^*(B)/m_N^*(0)$ of the effective nucleon Dirac mass in the magnetic field to its value in the absence of the field on baryon number density n in units of n_0 in the case of $NY\Delta$ composition. The result for the exponential field profile is shown by a solid and for universal by a dash-dotted line.

7.6 Summary

Recent years have seen substantial progress in describing compact stars with heavy baryons (hyperons as well as Δ-resonances) in a manner consistent with all the currently available astrophysical as well as laboratory data. Motivated by this, in this chapter we have extended one of the standard approaches which is based on RMF theory with density-dependent couplings to the case of strongly magnetized matter. In doing so, we have taken into account fully the Landau quantization of orbits of charged particles in strong fields. To quantify these effects we employed two parametrizations of the magnetic field profiles, namely the *exponential* and the *universal* profiles for a fixed value of the central magnetic field $B_c = 2.9 \times 10^{18}$ G. The universal profile implies a relatively high surface magnetic field of ∼5.6×10^{17} G and flat magnetic field profile. The exponential profile, by construction, is adjusted to produce a surface magnetic field value 10^{15} G. In this case, the profile is steep with the magnetic field changing by orders of magnitude. Having the profiles at hand, we have explored the changes in the composition of matter and the effective mass of the nucleon. We find typical

for magnetized system oscillations in these quantities which are similar to the de Haas-van Alphen oscillations of observables (e.g., the magnetic susceptibility of electronic systems) in magnetic fields. The oscillations have their origin in the occupation of the Landau levels by particles. As a result that the charged and neutral baryons are coupled by the baryon number and charge conservation, the oscillations are coupled as well and affect the fractions of neutral particles (neutrons, Λs and Δ^0s). The oscillations of the particle fractions are substantially different for the two profiles studied if they are compared for the same value of the central magnetic field. In the case of the universal profile, these oscillations extend up to the low-density regime because the field does not change substantially. In the exponential profile case, the low-density regime has low magnetic fields, therefore the amplitudes of oscillations are low. Comparing the oscillations in the strange and non-strange sectors we observe that the hyperon fractions are more affected by the magnetic fields that the non-strange baryon fractions within the density range considered. Furthermore, the Dirac nucleon effective masses exhibit similar oscillations, which implies that a range of quantities (specific heat, baryon mean-free-path, thermal conductivity, etc.) may show oscillations as well.